Konrad-Zuse-Zentrum
für Informationstechnik Berlin

Takustraße 7
D-14195 Berlin-Dahlem
Germany

BURKHARD SCHMIDT AND PETRA ŽĎÁNSKÁ [1]

Solution of the Time-Dependent Schrödinger Equation for Highly Symmetric Potentials [2]

[1]J. Heyrovský Institute of Physical Chemistry,
Academy of Sciences of the Czech Republic,
Dolejškova 3, 18223 Prague 8, Czech Republic

[2]to appear in: Computer Physics Communications

Preprint SC 99-11 (Nov 1999)

Abstract

The method of symmetry adapted wavepackets (SAWP) to solve the time–dependent Schrödinger equation for a highly symmetric potential energy surface is introduced. The angular dependence of a quantum–mechanical wavepacket is expanded in spherical harmonics where the number of close–coupled equations for the corresponding radial functions can be efficiently reduced by symmetry adaption of the rotational basis using the SAWP approach. Various techniques to generate symmetry adapted spherical harmonics (SASHs) for the point groups of highest symmetry (octahedral, icosahedral) are discussed. The standard projection operator technique involves the use of Wigner rotation matrices. Two methods to circumvent numerical instabilities occuring for large azimuthal quantum numbers are suggested. The first is based on a numerical scheme which employs Gaussian integrations yielding exact and stable results. The second is a recursive algorithm to generate higher order SASHs accurately and efficiently from lower order ones. The paper gives a complete set of "seed functions" generated by projection techniques which can be used to obtain SASHs for all irreducible representations of the octahedral and icosahedral point groups recursively.

1 Introduction

Point–group or space–group symmetry of molecular or crystallographic systems, respectively, can be exploited to greatly facilitate the solution of the time–independent (TISE) or time–dependent Schrödinger equation (TDSE). In almost all cases, symmetry adaption of wavefunctions is achieved by expanding wavefunctions in a symmetry adapted finite basis representation and solving the equations for the corresponding (stationary or dynamical) coefficients [1]. However, most of the recent work on quantum molecular dynamics [2–5] typically employs discrete variable representations (DVRs) in coordinate space [6,7]. In particular, Fourier collocation schemes as a special case of DVRs have become a widely used tool, owing to the favourable scaling properties of fast Fourier transforms (FFTs) [8–10]. Accordingly, symmetry adapted FFT methods [8, 11] as well as symmetry adapted DVRs [12] have been developed. These approaches have been limited so far to relatively low symmetries, e. g. the D_{3h} symmetry of the triatomic hydrogen reaction [11], the C_{2v} symmetry of the water molecule [13] or the D_{2h} symmetry of planar acetylene [14–16]. An extension of these approaches to point groups of highest symmetry such as the octahedral or icosahedral group poses severe difficulties. Whenever the symmetry involves more than a single (rotational) degree of freedom direct product of DVR schemes cannot be constructed in a straightforward manner.

The approach of symmetry adapted wavepackets (SAWPs) essentially represents a symmetry adaption of the well–known close coupled wavepacket

(CCWP) formalism [17, 18] where the angular dependence of a quantum mechanical wavepacket is expanded in terms of spherical harmonic (SH) functions Y_{jm} which is known to be more efficient than a pointwise DVR approach for spherical dynamics [19]. Inserting this approach into the TDSE yields a set of differential equations for the radial wavefunctions which are coupled through matrix elements of the potential energy. Because both the numerical effort and the storage requirement depend quadratically on the number of spherical harmonics used in the expansion scheme, it is highly desirable to reduce this number as far as possible. In the SAWP extension of the CCWP technique this is accomplished by the use of symmetry adapted spherical harmonics (SASHs) which transform according to irreducible representations of the point group of the Hamiltonian operator. This idea was first developed for the treatment of molecule–surface scattering [20,21]. However, those applications were confined to the case of cyclic or dihedral point groups where the construction of SASHs is relatively simple [22].

The present work aims at an extension of the SAWP technique to cases of highest symmetry, in particular to the octahedral and icoahedral point groups where the generation of SASHs is considerably more complicated. Another challenge of the present work stems from the requirement of large values of the azimuthal quantum number j. In contrast to electronic structure calculations, where only very low values of j play a role, typical quantum molecular dynamics simulations may require large values of j in the order of a few ten to a few hundred, see for example our wavepacket studies of HX (X=F, Cl) photodissociation inside octahedral (face–centered cubic) rare gas matrices [23] or inside icosahedral rare gas clusters [24,25].

The notion of SASHs for the octahedral point group O_h, which are often referred to as cubic, lattice, or surface harmonics, dates back to the very early stages of quantum mechanics. First approaches were made in ligand field theory [26–28] and in studies of the rotational motion of molecules in crystals [29, 30]. A more systematic approach can be found in work on electronic band structures [31]. Subsequently, improved schemes for the generation of SASHs were developed [32, 33] and SASHs for all irreducible representations of the point groups relevant in crystallography were compiled [22]. However, these tables are either limited to relatively low quantum states with $j \leq 12$ or to the totally symmetric irreducible representation A_{1g} of the O_h group [34].

The icosahedral point group I_h has been long neglected due to its irrelevance in conventional crystallography. Early exceptions are the works in Refs. [35] and [36]. Also in these cases the data are restriced to $j \leq 12$ or $j \leq 8$, respectively. Stimulated by new applications of the icosahedral symmetry in recent years in the fields of chemistry (fullerenes, e. g. C_{60}), solid state physics (quasi–crystals), and biology (viruses), icosahedral SASHs have been investigated in a number of recent publications [37–40]. However, the tabulated functions for $j \leq 30$ given in these studies are again restricted to the totally symmetric irreducible representation A_g of the I_h point group.

The standard technique of evaluating SASHs by means of projection operators involves the law of transformation of spherical harmonics using Wigner rotation matrices [22]. For the case of very large quantum numbers occuring in quantum molecular dynamics, severe numerical instabilities occur which limit the use of the standard method. In the present work, two approaches to circumvent these obstacles shall be followed. One of them is also based on projection operators but the evaluation of rotation matrices is avoided in a numerical approach based on Gaussian quadratures [41] which, in principle, allows exact and stable evaluation of SASHs. The other scheme used is a recursive algorithm to generate higher order SASHs from a very small set of low order functions, the so–called "seed functions". Originally it was only applied to the totally symmetric representation where it was shown to be both very accurate and very efficient [40]. In the present work this technique is extended to all representations of the octahedral and icosahedral point group.

The paper is organized as follows. The symmetry adapted wavepacket (SAWP) method is presented in the following Sec. 2. The various analytical and numerical approaches to generate symmetry adapted spherical harmonics (SASHs) are introduced in Sec 3. Results for the octahedral and icosahedral point group are given in Sec. 4. Finally, our conclusions are given in Sec. 5. An extensive appendix gives a complete set of "seed functions" for generation of SASHs for the two point groups under consideration.

2 Symmetry–Adapted Wavepackets

For a single particle of mass M in three–dimensional space, the time–dependent Schrödinger equation (TDSE) for the wavefunction ψ governed by a time–dependent potential V can be written in spherical coordinates r, θ, ϕ

$$i\hbar \frac{\partial}{\partial t}\psi(r,\theta,\phi,t) = \left[\frac{\hbar^2}{2M} \left(-\frac{1}{r}\frac{\partial^2}{\partial r^2} r + \frac{\hat{j}^2(\theta,\phi)}{r^2} \right) + V(r,\theta,\phi,t) \right] \psi(r,\theta,\phi,t) \tag{1}$$

where the first term on the r. h. s. stands for the radial part of the kinetic energy. The second term is the centrifugal interaction connected with the angular part of the kinetic energy which is represented here in terms of the angular momentum operator $\hat{j}$. Note that the TISE can be easily retrieved from the TDSE by simply replacing the l. h. s. of the above equation by $E\psi(r,\theta,\phi)$ and by omitting the time–dependence of potentials and wavefunctions.

In analogy with conventional close–coupling schemes to separate electronic and nuclear degrees of freedom, we treat angular and radial coordinates following the "close–coupled wavepacket" (CCWP) approach commonly used in diatom–surface scattering theory [17, 18], where the angular dependence of the 3–D wavefunction is expanded in a series of spherical harmonic functions

$$\psi(r,\theta,\phi;t) = \sum_{\Gamma\in G} \sum_{j=0}^{\infty} \sum_{n=1}^{N_j^{(\Gamma)}} \frac{\chi_{jn}^{(\Gamma)}(r,t)}{r} Z_{jn}^{(\Gamma)}(\theta,\phi) \tag{2}$$

where the time–dependent coefficients χ_{jn} can be identified as radial wavefunctions corresponding to each of the angular functions Z_{jn}. In this expansion it is assumed that the angular basis can be decomposed into sets of functions which transform according to irreducible representations Γ of the point group G given by the symmetry of the potential energy function. Note that the third summation extends over the $N_j^{(\Gamma)}$ SASHs of this representation for a given quantum number j. They are obtained as linear combinations of spherical harmonics Y_{jm} [22]

$$Z_{jn}^{(\Gamma)}(\theta,\phi) = \sum_{m=-j}^{j} c_{jnm}^{(\Gamma)} Y_{jm}(\theta,\phi), \quad n = 1\ldots N_j^{(\Gamma)} \quad , \tag{3}$$

the calculation of which will be detailed in the following section. Consequently, the SASHs are eigenfunctions of $\hat{j}^2$ but not of $\hat{j}_z$ any more. Note that the coefficients can always be chosen such that the SASHs are real–valued (see the Appendix). Inserting *ansatz* (2) into the TDSE (1) and projection on one of the angular SASH functions yields the following set of coupled equations

$$\begin{aligned} i\hbar\frac{\partial}{\partial t}\chi_{jn}^{(\Gamma)}(r,t) &= \frac{\hbar^2}{2M}\left[-\frac{\partial^2}{\partial r^2} + \frac{j(j+1)}{r^2}\right]\chi_{jn}^{(\Gamma)}(r,t) \\ &+ \sum_{j'=0}^{\infty}\sum_{n'=1}^{N_j^{(\Gamma)}} V_{jnj'n'}^{(\Gamma)}(r,t)\,\chi_{j'n'}^{(\Gamma)}(r,t) \end{aligned} \tag{4}$$

where the time evolution of the radial functions is determined by matrix elements of the potential energy surface in the SASH basis which are defined as integrals over the surface of the unit sphere with $d\Omega = \sin\theta\, d\theta\, d\phi$

$$V_{jnj'n'}^{(\Gamma)}(r,t) = \int d\Omega\, Z_{jn}^{(\Gamma)}(\theta,\phi)\, V(r,\theta,\phi,t)\, Z_{j'n'}^{(\Gamma)}(\theta,\phi) \quad . \tag{5}$$

Note that matrix elements of the potential energy function between SASHs belonging to different irreducible representations ($\Gamma' \neq \Gamma$) must vanish. It is convenient to expand the potential energy function in terms of SASHs of the totally symmetric representation ($\Gamma'' = \epsilon$)

$$V(r,\theta,\phi,t) = \sum_{j''=0}^{\infty}\sum_{n''=1}^{N_{j''}^{(\epsilon)}} U_{j''n''}(r,t)\, Z_{j''n''}^{(\epsilon)}(\theta,\phi) \quad . \tag{6}$$

The integrals to obtain the coefficients $U_{j''n''}$ are easier to calculate than a direct integration of Eq. (5) because an integrand of the form ZV has considerably fewer nodes than a triple product ZVZ. Now the matrix elements (5) of the potential energy can be written with the help of (3) as

$$
\begin{aligned}
V^{(\Gamma)}_{jnj'n'}(r,t) &= \sum_{j''=0}^{\infty} \sum_{n''=1}^{N^{(\epsilon)}_{j''}} U_{j''n''}(r,t) \sum_{m=-j}^{j} \sum_{m'=-j'}^{j'} \sum_{m''=-j''}^{j''} c^{(\Gamma)}_{jnm}\, c^{(\Gamma)}_{j'n'm'}\, c^{(\epsilon)}_{j''n''m''} \\
&\times \int d\Omega\, Y^{*}_{jm}(\theta,\phi)\, Y_{j'm'}(\theta,\phi)\, Y_{j''m''}(\theta,\phi) \quad . \qquad (7)
\end{aligned}
$$

The integral over triple products of spherical harmonics is readily evaluated with the help of the Clebsch–Gordan series [42]

$$
\begin{aligned}
\int d\Omega\, Y^{*}_{jm} Y_{j'm'} Y_{j''m''} &= (-1)^m \sqrt{\frac{(2j+1)(2j'+1)(2j''+1)}{4\pi}} \\
&\times \begin{pmatrix} j & j' & j'' \\ -m & m' & m'' \end{pmatrix} \begin{pmatrix} j & j' & j'' \\ 0 & 0 & 0 \end{pmatrix} \qquad (8)
\end{aligned}
$$

where (:::) represents the Wigner $3j$–symbol. As indicated by the order of the summations in Eq. (7), only the expansion coefficients $U(r,t)$ have to be calculated for every value of the radial coordinate and – in case of a time–dependent potential – for every time step, while the remaining three–fold sum and the $3j$–symbols have to be calculated only once for each irreducible representation Γ.

3 Symmetry Adapted Spherical Harmonics (SASHs)

3.1 Projection Operators

In this section we want to review different approaches to obtain symmetry adapted spherical harmonics (SASHs) $Z^{(\Gamma)}_{jn}(\theta,\phi)$ required for the expansion of the angular dependence of wavepackets, see Eqs. (2) and (3). We begin with the standard technique of forming symmetry adapted linear combinations of a set of basis functions using projection operators for a point group $\mathbf{G}$ consisting of $|\mathbf{G}|$ elements [1,43]. Irreducible representations Γ of dimension $l^{(\Gamma)}$ are characterized by matrix representations $\mathbf{D}^{(\Gamma)}(R)$ for each of the symmetry operations R. Given these representations it is straight–forward to obtain SASHs $Z^{(\Gamma)}_{jn}$ by applying the projection operators $\hat{W}^{(\Gamma)}_{ts}$ to spherical harmonics Y_{jn}

$$
\begin{aligned}
Z^{(\Gamma)}_{jn}(\theta,\phi) &= \hat{W}^{(\Gamma)}_{ts} Y_{jn}(\theta,\phi) \\
&= \frac{l^{(\Gamma)}}{|\mathbf{G}|} \sum_{R\in\mathbf{G}} \left[D^{(\Gamma)}(R)_{ts}\right]^{\star} \hat{R}\, Y_{jn}(\theta,\phi) \qquad (9)
\end{aligned}
$$

where it is sufficient to consider only the diagonal elements of the representation matrices into account ($t = s$). The basis functions obtained for each of the irreducible representations have to be orthogonalized using e. g. the standard Schmidt–Gram procedure.

The number of SASHs for a given value j belonging to each of the irreducible representations i can be easily obtained by decomposing the $2j+1$ dimensional representation of the spherical group

$$N_j^{(\Gamma)} = \frac{1}{|\mathbf{G}|} \sum_{R\in\mathbf{G}} \left[\chi^{(\Gamma)}(R)\right]^\star \chi_j(R) \tag{10}$$

where $\chi^{(\Gamma)}(R) = \sum_t D^{(\Gamma)}(R)_{tt}$ is the character of the irreducible representation. The characters $\chi_j(R)$ are obtained as [26]

$$\chi_j(R) = P_R \frac{\sin\left[(j+\frac{1}{2})\Phi_R\right]}{\sin\left[\frac{1}{2}\Phi_R\right]} \tag{11}$$

where each symmetry operation R is considered either as a single rotation by an angle Φ_R or as a rotation followed by an inversion, giving rise to $P_R = 1$ or $P_R = (-1)^j$, respectively.

The above relation to generate SASHs is simple when applied to low symmetries such as the cyclic or dihedral groups or when only low values of the angular momentum j are considered. For example, the use of symmetry adapted orbitals is routinely implemented in standard electronic structure calculation codes. However, its use in quantum molecular dynamics is hampered by the need for higher angular momenta due to the much larger masses of the nuclei. In the following subsections, different methods to evaluate (9) are introduced and their capability to generate SASHs for the icosahedral and octahedral point group and for high j values is reviewed.

3.2 Projection Method Using Rotation Matrices

The standard method to calculate SASHs is based on the law of transformation of spherical harmonics [42,44,45] to solve Eq. (9). The transformation under the various symmetry operations R forming the group G results in a coupling of different m-sublevels of the same angular momentum j

$$\hat{R}Y_{jn}(\theta,\phi) = \sum_{m=-j}^{j} P_R \mathcal{D}_{jnm}(\alpha_R,\beta_R,\gamma_R) Y_{jm}(\theta,\phi) \tag{12}$$

where the rotation R is parametrized by the Euler angles $\alpha_R, \beta_R, \gamma_R$. Inserting the above equation into Eq. (9) and comparing with Eq. (3) yields expressions for the coefficients of the SASHs in terms of spherical harmonics

$$c_{jnm}^{(\Gamma)} = \frac{l^{(\Gamma)}}{|\mathbf{G}|} \sum_{R\in\mathbf{G}} \left[D^{(\Gamma)}(R)_{ts}\right]^\star P_R \mathcal{D}_{jnm}(\alpha_R,\beta_R,\gamma_R) \quad . \tag{13}$$

The Wigner rotation matrices $\mathcal{D}_{jnm}$ can be expressed as [22,42,44]

$$\mathcal{D}_{jnm}(\alpha,\beta,\gamma) = \begin{cases} \quad \exp[-im(\alpha+\gamma)]\delta_{n,m} & \beta = 0 \\ (-1)^j \quad \exp[-im(\alpha-\gamma)]\delta_{n,-m} & \beta = \pi \\ (-1)^f \quad \exp[-i(m\alpha+n\gamma)]d_{jnm}(\beta) & \text{else} \end{cases} \tag{14}$$

with $f = |n| + n - |m| - m$. While for simple point groups such as the cyclic and dihedral groups the frame of reference can always be chosen such that all symmetry operations can be described by a (proper or improper) rotation by $\alpha + \gamma$ or $\alpha - \gamma$ about the z–axis (for $\beta = 0$ or $\beta = \pi$, respectively) this is not the case for the octahedral and icosahedral point groups where – due to the three–, four, and five–fold axes – also other values of β occur. Then it becomes necessary to evaluate the reduced matrices which are given by

$$\begin{aligned} d_{jnm}(\beta) &= \sqrt{(j+n)!(j+m)!(j-n)!(j-m)!} \\ &\times \sum_{k=max(0,m-n)}^{min(j-n,j+m)} \\ &\times \frac{(-1)^k}{(j-n-k)!(j+m-k)!(k-m+n)!k!} \\ &\times \cos\left(\frac{\beta}{2}\right)^{2j+m-n-2k} \sin\left(\frac{\beta}{2}\right)^{2k+n-m} \quad . \end{aligned} \tag{15}$$

Using an 8–byte representation for floating point numbers, both a direct logarithmic calculation and a calculation by means of a recursion relation given in Ref. [22] were found to be stable only up to $j \approx 40 \ldots 45$ for the octahedral and the icosahedral point group. Very recently novel recursion relations for the construction of rotation matrices have been derived which appear to be considerably more efficient and numerically stable [46].

3.3 Projection Method Using Numerical Integration

A practical alternative to calculate SASHs by projection operator methods avoiding the use of Wigner rotation matrices and the problems occuring for the evaluation of products and fractions of factorials in Eq. (15) is introduced in Ref. [41]. This method is based on Gaussian integrations and lends itself more easily to implementation on computers. First of all, it is straightforward to obtain the SASH coefficients $c_{jnm}^{(\Gamma)}$ defined in Eq. (3) by projecting SASHs as given by Eq. (9) on a spherical harmonic Y_{lm}

$$c_{jnm}^{(\Gamma)} = \frac{l^{(\Gamma)}}{|\mathbf{G}|} \sum_{R \in \mathbf{G}} \left[D^{(\Gamma)}(R)_{ts} \right]^* \int d\Omega \, Y_{jm}^*(\theta,\phi) \, \hat{R} \, Y_{jn}(\theta,\phi) \quad . \tag{16}$$

Subsequently, the use of Wigner rotation matrices to evaluate $\hat{R} \, Y_{jn}(\theta,\phi)$ can be avoided by simply replacing the action of the symmetry operation $\hat{R}$

on the spherical harmonics by its reverse $\hat{R}^{-1}$ acting on the arguments of the spherical harmonic

$$\hat{R}\,Y_{jn}(\theta,\phi) = Y_{jn}\left(\hat{R}^{-1}(\theta,\phi)\right) \quad . \tag{17}$$

Following the work of Ref. [41], it is easy to show how the above integrals can be calculated in a numerically exact manner using a direct product of two Gaussian quadrature schemes. According to the law of transformation of spherical harmonics (12) it is evident that the integrals must be linear combinations of terms of the form

$$\sim \int_{-1}^{1} d(\cos\theta)\, P_{jm}(\cos\theta)\, P_{jn}(\cos\theta) \int_{0}^{2\pi} d\phi\, e^{i(n-m)\phi} \tag{18}$$

where P_{jm}, P_{jn} are the associated Legendre polynomials. Although the coefficients of the linear combinations are not explicitly known, consideration of (18) is helpful to characterize the integrand of (16) and to choose appropriate quadrature schemes for the numerical integration of (16). The integrand is a polynomial of the order $2j$ in the argument $\cos\theta$ and can be evaluated exactly using a Gauss-Legendre scheme with $j+1$ quadrature points. The integration over ϕ is carried out using equally spaced abscissae thus projecting out the $m = n$ component. By analogy with the Nyquist theorem for discrete Fourier transforms it can be shown that $2j+1$ integration points are necessary and sufficient to obtain a numerically exact result for (16).

3.4 Recursive Method

A very elegant way to circumvent the tedious numerical calculation of the two projection operator methods presented above is suggested in Ref. [40] where a recursive algorithm to generate higher order SASHs which transform according to representation Γ from products of lower order SASHs ('seed functions') is developed. Whenever the direct product of two irreducible representations Γ' and Γ'' contains only the desired representation Γ

$$\Gamma' \otimes \Gamma'' \;=\; \Gamma \tag{19}$$

it follows from group theory that any product of SASHs belonging to Γ' and Γ'' can be written in terms of SASHs transforming according to representation Γ

$$Z^{(\Gamma')}_{j'n'}(\theta,\phi)\, Z^{(\Gamma'')}_{j''n''}(\theta,\phi) \;= \sum_{j=0}^{\infty} \sum_{n=1}^{N_j^{(\Gamma)}} k^{(\Gamma,\Gamma',\Gamma'')}_{jnj'n'j''n''}\, Z^{(\Gamma)}_{jn}(\theta,\phi) \tag{20}$$

where the coefficients k characterize the linear combinations. Inserting the definition of SASHs (3) on both sides of the equation provides a relation between the coefficients $c^{(\Gamma')}, c^{(\Gamma'')}$ of the seed functions, which are assumed to be known, and the unknown coefficients $c^{(\Gamma)}$ of the wanted function $Z_{jn}^{(\Gamma)}$

$$\sum_{m'=-j'}^{j'} \sum_{m''=-j''}^{j''} c_{j'n'm'}^{(\Gamma')} \, c_{j''n''m''}^{(\Gamma'')} \, Y_{j'm'} \, Y_{j''m''} =$$

$$= \sum_{j=0}^{\infty} \sum_{n=1}^{N_j^{(\Gamma)}} k_{jnj'n'j''n''}^{(\Gamma,\Gamma',\Gamma'')} \sum_{m'''=-j'''}^{j'''} c_{jnm'''}^{(\Gamma)} \, Y_{jm'''} \quad . \tag{21}$$

Next, this equation is projected by on the spherical harmonic Y_{jm} where Eq. (8) is used to evaluate the left hand side, respectively

$$\sum_{m'=-j'}^{j'} \sum_{m''=-j''}^{j''} c_{j'n'm'}^{(\Gamma')} \, c_{j''n''m''}^{(\Gamma'')} \, (-1)^m \sqrt{\frac{(2j+1)(2j'+1)(2j''+1)}{4\pi}} \times$$

$$\times \begin{pmatrix} j & j' & j'' \\ 0 & 0 & 0 \end{pmatrix} \begin{pmatrix} j & j' & j'' \\ -m & m' & m'' \end{pmatrix} = \sum_{n=1}^{N_j^{(\Gamma)}} k_{jnj'n'j''n''}^{(\Gamma,\Gamma',\Gamma'')} \, c_{jnm}^{(\Gamma)} \quad . \tag{22}$$

Note that it is helpful to consider the conditions for non–vanishing Wigner $3j$ symbols. The triangle rule $|j'-j''| \le j \le j'+j''$ imposes certain restrictions on the choice of functions Z_{jn} that can be constructed from a given pair of seed functions for j' and j'' (see below). Moreover, the second of the $3j$ symbols is only non–zero for $-m+m'+m''=0$ which can be used to omit the m''–summation. After including all m–independent terms into a new proportionality constant κ one finally obtains

$$\sum_{m'} c_{j'n'm'}^{(\Gamma')} \, c_{j''n''m-m'}^{(\Gamma'')} \, (-1)^m \begin{pmatrix} j & j' & j'' \\ -m & m' & m-m' \end{pmatrix} = \sum_{n=1}^{N_j^{(\Gamma)}} \kappa_{jnj'n'j''n''}^{(\Gamma,\Gamma',\Gamma'')} \, c_{jnm}^{(\Gamma)} \tag{23}$$

where the summation over m' extends from $\max(-j', -j''+m)$ to $\min(j', j''+m)$. If there exists only one SASH function ($N_j^{(\Gamma)} = 1$) for given angular momentum j and given representation Γ then it is straightword to obtain an expression for the coefficients $c_{jnm}^{(\Gamma)}$ by simply identifying κ as a normalization constant of Z_{jn}. In case of degenerate SASHs the above equation has to be evaluated for a set of $N_j^{(\Gamma)} > 1$ different pairs of seed functions j', n', j'', n'' which are compatible with the choice of j, n. Subsequently, the resulting coefficient vectors in m for different n have to be orthogonalized and normalized.

4 SASHs for the octahedral and icosahedral point groups

4.1 Number of SASHs

Before turning to the details of the calculation of the SASHs in the following subsections we would first like to discuss the number of SASHs for the irreducible representations of the octahedral (O_h) and icosahedral (I_h) point group. These numbers are obtained as the number of times a certain representation occurs upon decomposition of the $(2j+1)$–fold degenerate representations of the spherical group, see Eq. (10).

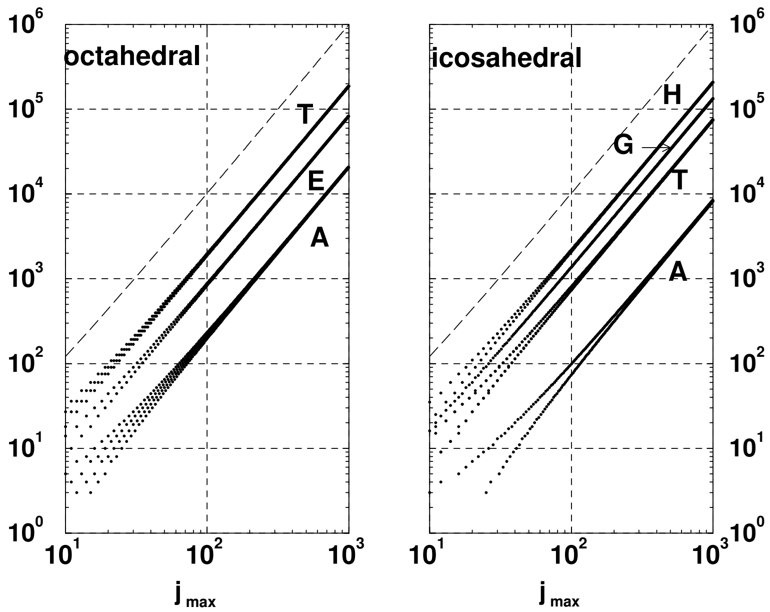

Figure 1: Cumulative number $N_S^{(\Gamma)}(j_{\max})$ of symmetry adapted spherical harmonics. The solid curves are for all representations of the octahedral (left) and icosahedral (right) point group. In the limit of large values of j, the curves approach $j_{\max}^2(l^{(\Gamma)})^2/|\mathbf{G}|$, see Eq. (24). For comparison, the dashed curve gives the size $N_N(j_{\max})$ of a basis of non–symmetry adapted spherical harmonics.

Fig. 1 shows our results for the case of the I_h group. The curves indicate the accumulated numbers of SASH functions $N_S^{(\Gamma)}(j_{\max}) = \sum_{j=0}^{j_{\max}} N_j^{(\Gamma)}$ where $j_{\max}$ indicates the maximum possible angular momentum considered and $N_j^{(\Gamma)}$ is calculated from (10). These numbers have to be compared with the number of non–symmetry adapted spherical harmonics $N_N(j_{\max}) = \sum_{j=0}^{j_{\max}}(2j+1) = (j_{\max}+1)^2$. In the limit of large angular momentum quantum numbers j, the number of SASHs scales with

$$\lim_{j\to\infty} N_S^{(\Gamma)}(j_{\max}) = \frac{j_{\max}^2 (l^{(\Gamma)})^2}{|\mathbf{G}|} \tag{24}$$

where $l^{(\Gamma)}$ is the dimensionality of the representation Γ and $|\mathbf{G}|$ is the number of symmetry operations forming the point group. For the point groups considered here, we have $|\mathbf{G}| = 48$ for O_h and $|\mathbf{G}| = 120$ for I_h. In the most favorable case of the one–dimensional representations A_g/A_u of the point group I_h, the number $N_S^{(\Gamma)}$ of SASHs is more than two orders of magnitude less than the number N_N of spherical functions in the non–symmetric case. This ratio becomes less favorable in the case of the higher–dimensional representations. However, even in the worst case of the five–dimensional H_g/H_u representations, the number of functions is reduced by a factor of 24/5.

Consequently, the number of coupled equations in (4) that have to be solved simultaneously is greatly reduced which is the key advantage of the SAWP technique for point groups of high symmetry. In particular, both the numerical effort of the Hamiltonian operation and the storage required for the potential energy matrix scale quadratically with $N_S^{(\Gamma)}$. If the coupled equations are to be solved by methods relying on a diagonalization of the matrix representation (5) of the potential energy [47], the effort scales with the third power of $N_S^{(\Gamma)}$. These considerations clearly show the dramatic improvement of the SAWP method in comparison with an un–symmetrized CCWP approach.

4.2 Generation of totally symmetric SASHs

The use of the recursive method as shown in Eq. (23) is demonstrated in Ref. [40] for the totally symmetric irreducible representation $\Gamma = \Gamma' = \Gamma'' = \epsilon$. For the special case of the icosahedral point group (I_h) we have $\epsilon = A_g$. Clearly the first of the SASHs which transforms according to this representation is the trivial function ($j = 0$). In principle, only the second A_g functions (j=6, see also Tab. 1) is needed as a seed function. From a combination of this function with itself ($j' = j'' = 6$), the third function ($j = 10$) can be generated. For the generation of the fourth SASH ($j = 12$) there are already two possibilities, one with $j' = j'' = 6$ and one with $j' = 10, j'' = 6$. For higher functions there is a rapidly increasing number of possibilities of different combinations of quantum number j', j'' to generate functions for a given value of j.

Instead, we suggest to use the first two non–trivial totally symmetric SASHs as seed functions which have to be generated by projection operator techniques. These are the $j' = 4$ and $j'' = 6$ SASHs for the O_h group [22] (see Tab. 1) and the $j' = 6$ and $j'' = 10$ SASHs for the I_h group [35] (see Tab. 7), which can be used as seed functions to construct higher order functions as combinations of the kind

$$j = sj' + tj'', \quad s, t \geq 0 \tag{25}$$

This approach is very convenient for the following two reasons. First, one always obtains the correct multiplicities when considering all combinations of integer numbers s, t leading to a given value of j. For the example of the icosahedral group, there is a unique possibility to generate SASHs for $j = 12, 16, 18, 20, 22, 24, 26, 28$. The two–fold degeneracy for $j = 30$ is correctly reproduced by the two combinations $5, 0$ and $0, 3$ for s and t, and so forth. Secondly, for the (repeated) evaluation of Eq. (23) with $j = j' + j''$ the triangle formed by the angular momentum vectors corresponding to j, j', j'' becomes a stretched triangle [40] with parallel edges which offers the advantage of a simplified calculation of the Wigner $3j$–symbol in (23) by means of [45]

$$\begin{pmatrix} j'+j'' & j' & j'' \\ -m & m' & m-m' \end{pmatrix} = (-1)^{j'-j''+m} \times \sqrt{\frac{(2j')!(2j'')!(j'+j''+m)!(j'+j''-m)!}{(2j'+2j''+1)!(j'+m')!(j'-m')!(j''+m-m')!(j''-m+m')!}} \tag{26}$$

Fig. 2 illustrates the two lowest non–trivial ($j > 0$) totally symmetric SASHs of the octahedral and the icosahedral point group. The structure of the densities $|Z_{jn}^{(\epsilon)}|^2$ follows a similar scheme which becomes obvious when considering the nodal pattern for each of the triangles comprising the platonic body. The first function ($j = 4$ for O_h, $j = 6$ for I_h) exhibits one class of extrema at each of the corners and another class of extrema (with different sign of $Z_{jn}^{(\epsilon)}$) at the center of each of the faces. In contrast, the next higher functions ($j = 6$ for O_h, $j = 10$ for I_h) have their main extrema at the centers of each of the edges.

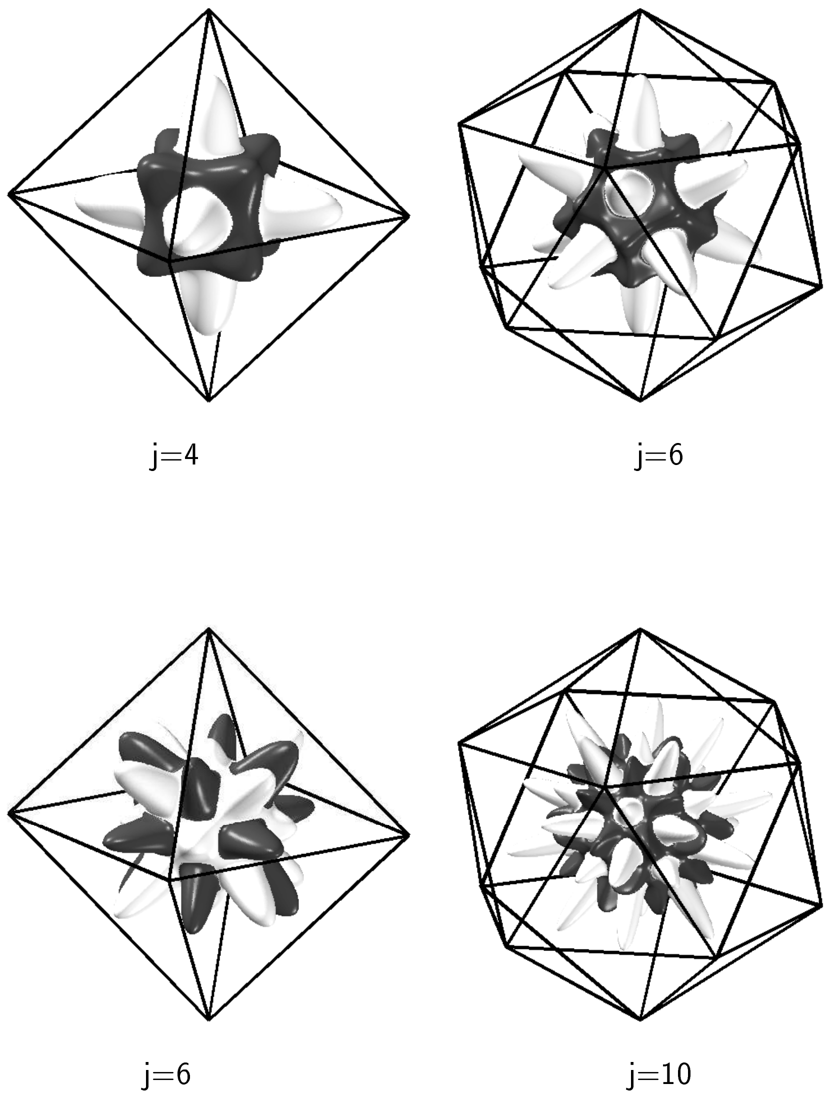

Figure 2: Two lowest SASH functions transforming according to the totally symmetric irreducible representation ϵ of the octahedral (O_h, A_{1g}, left panel) and icosahedral (I_h, A_g, right panel) point group. The radius of the spherical plots represents the density Z^2 added to a constant. The sign of Z is represented by the dark or light color. Note that these functions are used as seed functions to generate all higher SASHs for the totally symmetric representations with the help of Eq. (25).

4.3 Generation of remaining SASHs

For the construction of the SASHs transforming according to the non–totally symmetric irreducible representations we proceed similarly as for the totally symmetric representation ϵ. We make use of the fact that the direct product of ϵ with any representation yields the latter one

$$\epsilon \otimes \Gamma = \Gamma \tag{27}$$

which is a special case of Eq. (19). Hence, we choose as seed vectors a set containg all of the SASHs of ϵ–symmetry which are assumed to have been generated previously and augment it by as few as posssible SASHs of the representation Γ which have to be generated using the projection operator method. Then the whole set of SASHs $Z_{jn}^{(\Gamma)}$ can be generated from a combination of each of the $Z_{j'n'}^{(\epsilon)}$ with each of the additional seed functions $Z_{j''n''}^{(\Gamma)}$ applying again the rule of the stretched triangle ($j = j' + j''$) using (23) and (26). As in the case of the totally symmetric SASHs, this procedure guarantees the correct multiplicity of the generated functions $Z_{jn}^{(\Gamma)}$. It is noted that the seed functions for $\Gamma \neq \epsilon$ are not always the SASHs with the lowest possible value of j. For instance, it is found that three triples of seed functions with $j'' = 6, 10, 14$ are necessary and sufficient for the recursive calculation of all SASHs for the T_{1g} representation of the icosahedral point group which are triples of SASH functions with $j = 6, 10, 12, 14, 16, 16, 18, 20, 20, 22, 22, \ldots$, see also Tab. 9.

In general, we find that $(l^{(\Gamma)})^2$ additional seed functions are necessary and sufficient to generate all of the wanted SASHs $Z_{jn}^{(\Gamma)}$ for an irreducible representation of dimension $l^{(\Gamma)}$ using the stretched triangle rule (26). This set of functions can be decomposed into $l^{(\Gamma)}$ different subsets where the functions for a given j form a multiplet consisting of a single member of each of the mutually orthogonal subsets. In practice, these subsets can be easily identified by the different m–values of the non–vanishing coefficients $c_{jnm}^{(\Gamma)}$ and/or by the cos–like or sin–like ϕ–dependence, see our remarks in the Appendix. It is noted that these subsets can be correlated with irreducible representations of certain subgroups of the octahedral or icosahedral group. For instance, the two subsets of E_g SASHs of the O_h group can be identified with the A_{1g} and B_{1g} representation of the D_{4h} group, while the T_{1g} representation of the O_h group correlates with A_{2g} and E_g of D_{4h}.

Because the subsets of seed functions of a given representation Γ remain disjoint upon multiplication with a totally symmetric function $Z_{jn}^{(\epsilon)}$, also the total set of SASHs for a given multi–dimensional representation can be grouped into $l^{(\Gamma)}$ subsets with $N_S^{(\Gamma)}/l^{(\Gamma)}$ members. Because the matrix elements (5) of the potential energy between SASHs belonging to different subsets vanish, the number of coupled equations (4) can be reduced by a factor of $l^{(\Gamma)}$, see also our conclusions in Sec. 5.

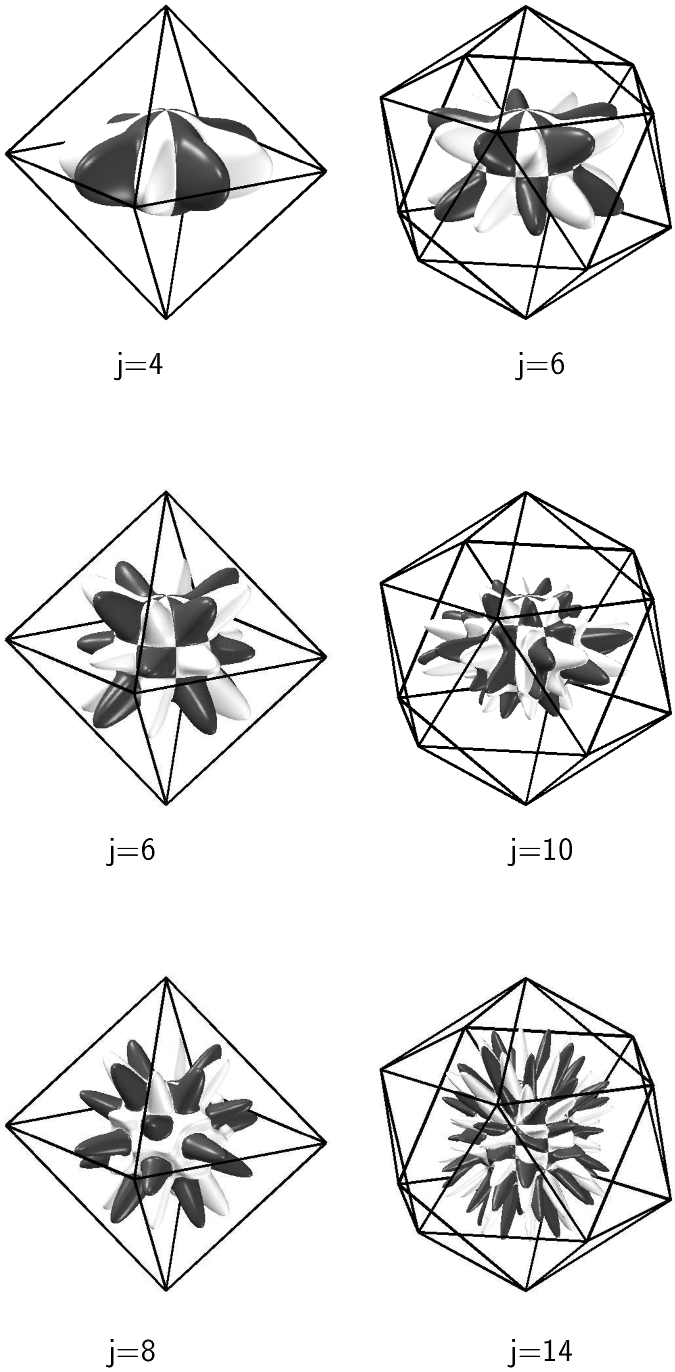

Figure 3: Three lowest SASH functions transforming according to the three–dimensional irreducible representation T_{1g} of the octahedral (O_h, left) and icosahedral (I_h, right) point group. Together with the totally symmetric ϵ–SASHs these functions can be used as seed functions to generate all higher SASHs of the T_{1g}–symmetry with the help of Eq. (27)

The procedure described above is followed for all representation of even (g) inversion symmetry, i. e. those whose characters are positive for inversion and improper rotations. All the necessary seed functions are listed in Tabs. 3 through 6 for the octahedral point group and in Tabs. 9 through 12 for the icosahedral point group. As an example, the seed functions of one of the three–dimensional representations (T_{1g}) of both the O_h and I_h point group are illustrated in Fig. 3. It is noted that the rotation about the axes of highest order transforms according to this representation. Accordingly, the SASHs are of 4–fold (O_h) or of 5–fold (I_h) rotational symmetry. Perpendicular to this axis, there is a stack of $0, 2, 4$ nodal planes for the $j = 4, 6, 8$ functions of the octahedron or $1, 5, 9$ nodal planes for the $j = 6, 10, 14$ functions of the icosahedron.

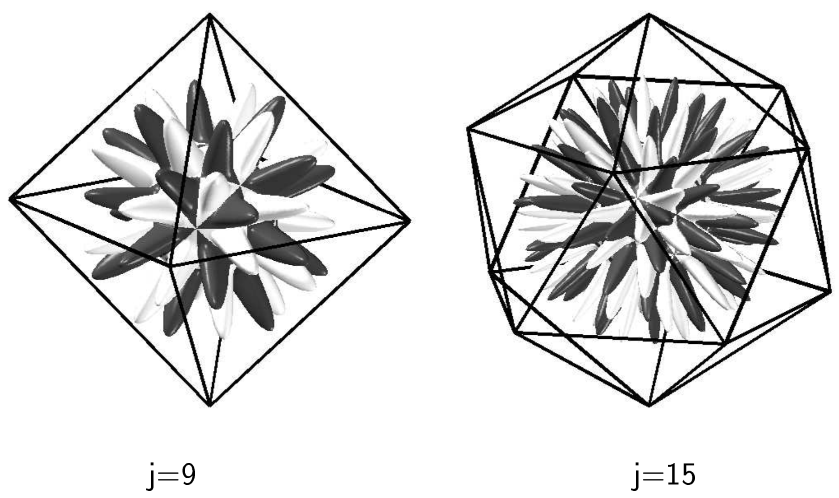

Figure 4: Lowest SASH functions transforming according to the ζ irreducible representation of the octahedral (O_h, A_{1u}, left) and icosahedral (I_h, A_u, right) point group. Together with the totally symmetric ϵ–SASHs these functions can be used as seed functions to generate all higher SASHs of the respective ζ–symmetry with the help of Eq. (28)

A particularly simple way to generate all the SASHs for the representations of the odd (u) inversion symmetry is given by the direct product

$$\zeta \otimes \Gamma_g = \Gamma_u \tag{28}$$

where ζ is the u–representation (odd parity) corresponding to the totally symmetric one, i. e. A_{1u} for the O_h group and A_u for the I_h group. First of all, this equation allows to generate ζ–SASHs by identifying $\Gamma_g = \epsilon$ and $\Gamma_u = \zeta$. This can be achieved by combining only one additional seed function $Z^{(\zeta)}_{j'n'}$ with each of the SASHs of the totally symmetric representation $Z^{(\epsilon)}_{j''n''}$. For the point groups considered here, the additional seed functions are found to be the lowest order SASHs for the ζ representation, i. e. $j' = 9$ for O_h (see Tab. 2) and $j' = 15$ for I_h (see Tab. 8). All the remaining functions $Z^{(\zeta)}_{jn}$ can again be obtained by the stretched triangle rule $j' + j'' = j$. The additional seed functions are illustrated in Fig. 4. The corresponding densities $|Z^{(\zeta)}_{jn}|^2$ are totally symmetric, but the arrangement of minima and maxima of $Z^{(\zeta)}_{jn}$ is such that they interchange upon inversion.

Once the ζ functions are found, it is straightforward to construct the SASHs for the remaining representations Γ_u by combining any of the $Z^{(\zeta)}_{j'n'}$ with the seed functions $Z^{(\Gamma_g)}_{j''n''}$ discussed above to give the unknown SASHs $Z^{(\Gamma_u)}_{jn}$. In this case a complete and unique set of combinations is found for $j' - j'' = j$. For the example of the icosahedral point group I_h, the A_u function ($j' = 15$) can be combined with the T_{1g} seed functions ($j'' = 6, 10, 14$) to yield a complete set of T_{1u} seed functions for $j = 1, 5, 9$.

4.4 Numerical Considerations

The computational effort for the generation of SASHs using the recursive method [40] is illustrated in Fig. 5 where we restrict ourselves to the example of the icosahedral point group. The computational time has been measured on a HP A 9000/782 workstation computer. The details are closely connected to the procedure described in Sec. 4.2 and with our algorithmic realization which consists of three independent steps. First, totally symmetric SASHs (A_g representation) are generated using only the first seed function. We apply Eqs. (23) and (26) recursively in order to evaluate (25) for $j = 6s, s = 1, 2, \ldots$ assuming $j' = 6(s-1)$, $j'' = 6$. Analogously, another set of SASHs is generated from the second seed vector ($j = 10s$). The effort to generate these sets was found to scale with $\mathcal{O}(j)$. Finally, the set of SASHs for the A_g representation is completed by considering all combinations of the two sets, see Eq. (25). In the limit of large values of j the degeneracy $N^{(\Gamma)}_j$ is proportional to j and the effort to evaluate (23) scales approximately with $\mathcal{O}(j^2)$. Fig. 2 shows also the computer time to generate SASHs transforming according to other irreducible representations of the I_h group. The function for the T_{1g} representation are obtained applying Eq. (27), those for the A_u representation by virtue of Eq. (28). The effort to calculate these functions from a given set of seed functions is again found to scale with j^2 with prefactors reflecting the higher degeneracy $N^{(\Gamma)}_j$ of SASHs for multi–dimensional irreducible representations.

For comparison, Fig. 5 also displays the computational effort to generate

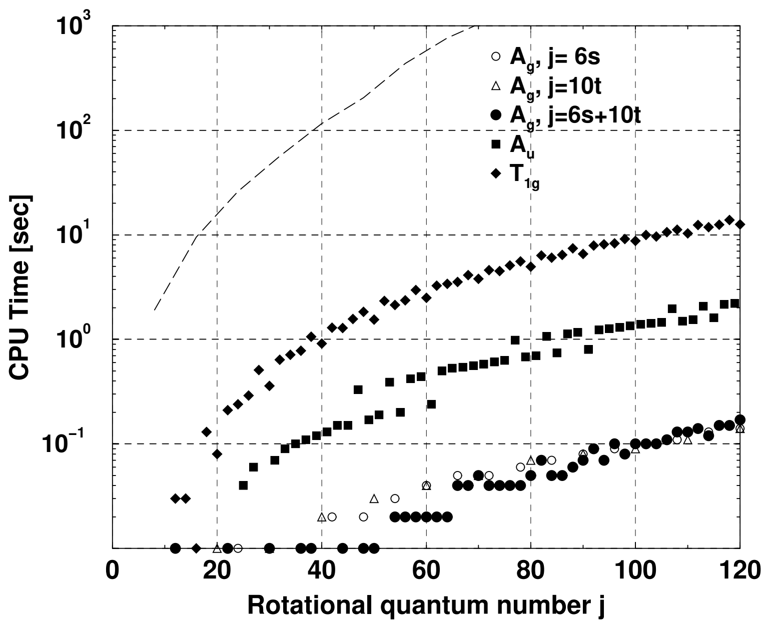

Figure 5: Computational effort for the generation of SASHs by the recursive method [40] for selected representations (A_g, A_u, T_{1g}) of the icosahedral point group (I_h). Details of the generation of the A_g function from multiples of $j' = 6$ and $j'' = 10$ are given in the text, see also Eq. (25). For comparison, the dashed curve shows the effort to generate the A_g function by the projection operator method using numerical integration [41].

totally symmetric SASHs (I_h, A_g) by the projection operator method using numerical integrations [41]. It is found that the required computer time exceeds the effort of the recursive method by approximately two orders of magnitude for the range of j considered in the figure. The most time-consuming step (more than 90% of CPU time) for the integration method stems from the calculation of spherical harmonics (SHs). Since the algorithm involves the integration over products of two SHs using two–dimensional grids in θ and ϕ the number of evaluations of these functions scales with $\mathcal{O}(J^2)$. We use a modified version of the routine given in Ref. [48] which calculates SHs for all m and for given j and for given arguments θ, ϕ. Hence, the effort is proportional to $\mathcal{O}(J^2)$ so that the total effort of the method exhibits a $\mathcal{O}(J^4)$ scaling behaviour.

5 Conclusions

The technique of symmetry adapted wavepackets (SAWP) represents a highly effective technique to solve the Schrödinger equation for highly symmetric potentials in three–dimensional space. In principle the computational effort is determined by the two ingredients of the method. (1) Using the close–coupling wavepacket (CCWP) *ansatz* both the numerical effort to solve the coupled equations and the storage requirement for the potential energy matrix scale with $N_N^2 \times N_R$ where $N_N = (j_{\max} + 1)^2$ stands for the number of spherical harmonics occuring in the expansion of the angular part of the wavefunction and N_R is the number of points in a collocation scheme typically used to represent the radial wavefunctions. This may be compared with the cartesian approach using a direct product of collocation schemes in each of the three degrees of freedom where the storage requirement for the wavefunction scales with N_R^3. Hence, the CCWP scheme is numerically advantageous only for applications with relatively low values of the angular momentum ($j_{\max} << \sqrt{N_R}$). (2) If the potential energy function (and hence the total Hamiltonian) of the system is symmetric, the efficiency can be greatly improved by symmetry adaption of the angular functions to yield symmetry–adapted spherical harmonics (SASHs). If the initial state transforms according to one of the irreducible representations of the point group of the Hamiltonian, the number of coupled equations in the CCWP scheme can be reduced by a factor of $|\mathbf{G}|/(l^{(\Gamma)})^2$ where $|\mathbf{G}|$ is the number of symmetry operations and $l^{(\Gamma)}$ represents the dimensionality of the representation Γ. Under favorable circumstances, i. e. when the initial state can be assigned to one of the subsets of the set SASHs for a multi–dimensional representation Γ, the number of basis functions can be further decreased by a factor of $l^{(\Gamma)}$. For point groups of very high symmetry such as the octahedral and icosahedral group, this reduction of the size of the basis set can be about one or two orders of magnitude thus making the approach also attractive for higher values of the maximum angular momentum. With the condition

$$j_{\max} << \sqrt{\frac{N_R|\mathbf{G}|}{l^{(\Gamma)}}} \quad . \tag{29}$$

being valid, the SAWP method emerges to be a valuable tool in the field of quantum molecular dynamics. First applications can be found in the quantum molecular dynamics simulations of photodissociation of hydrogen–containing diatomic molecules in the environment of icosahedral clusters or octahedral matrices [23–25].

Furthermore, the present paper has addressed the question of the generation of spherical harmonics for very high values of the angular momentum quantum number ($j >> 100$) and for the octahedral and icosahedral point groups which were not available in the previous literature. In particular, it has been shown that the recursive method is far superior to the methods based on projection operators, i. e. both the standard method using Wigner rotation matrices and a newer version relying on numerical integrations. However, these two methods are useful to generate low order seed functions needed to initialize the recursive method. Complete tables of seed functions for all irreducible representations of the O_h and I_h groups investigated in the present work are given in the Appendix. They allow accurate and efficient generation of higher order SASHs by means of the recursive method.

Acknowledgements

The authors would like to thank P. Jungwirth (Heyrovský Institute, Prague) for useful discussions and F. Neugebauer (Humboldt University, Berlin) for a computer code to calculate the SASHs by means of the standard technique using rotation matrices [22]. The illustrations of symmetry adapted spherical harmonic functions have been created by Ch. Salzmann at the ZIB. Financial support by the Volkswagen foundation through grant No. I/72114 is acknowledged.

References

[1] M.Tinkham. *Group Theory and Quantum Mechanics.* McGraw-Hill, New York, 1964.

[2] K. C. Kulander, editor. *Special Issue on Time-Dependent Methods for Quantum Dynamics*, volume 63 of *Comp. Phys. Commun.*, 1991.

[3] R. E. Wyatt and J. Z. H. Zhang, editors. *Dynamics of Molecules and Chemical Reactions*, New York, 1996. Dekker.

[4] W. Domcke, P. Hänggi, and D. Tannor, editors. *Special Issue on Dynamics of Driven Quantum Systems*, volume 217 of *Chem. Phys.*, 1997.

[5] J. Manz. Molecular wavepacket dynamics: Theory for experiments 1926–1996. In V. Sundström, editor, *Femtochemistry and Femtobiology: Ultrafast Reaction Dynamics at Atomic–scale Resolution*, pages 80–318. Imperial College Press, London, 1997.

[6] J. V. Lill, G. A. Parker, and J. C. Light. Discrete variable representations and sudden models in quantum scattering theory. *Chem. Phys. Lett.*, 89:483, 1982.

[7] J. C. Light, I. P. Hamilton, and J. V. Lill. Generalized discrete variable approximation in quantum mechanics. *J. Chem. Phys.*, 82:1400, 1985.

[8] M. D. Feit, J. A. Fleck, Jr, and A. Steiger. Solution of the Schrödinger equation by a spectral method. *J. Comput. Phys.*, 47:412, 1982.

[9] R. Kosloff. Time-dependent quantum-mechanical methods for molecular dynamics. *J. Phys. Chem.*, 92:2087, 1988.

[10] R. Kosloff. Propagation methods for quantum molecular dynamics. *Annu. Rev. Phys. Chem.*, 45:145–178, 1994.

[11] Y. Shi and D. J. Tannor. Symmetry adapted Fourier solution of the time–dependent Schrödinger equation. *J. Chem. Phys.*, 92(4):2517–2525, 1990.

[12] R. M. Whitnell. Symmetry–adapted discrete variable representation. *J. Chem. Phys.*, 89(6):3674–3680, 1988.

[13] Z. Bacic, D. Watt, and J. C. Light. A variational localized representation calculation of the vibrational levels of the water molecule up to 27 000 cm^{-1}. *J. Chem. Phys.*, 89(2):947–955, 1988.

[14] L. Liu and J. T. Muckerman. Vibrational eigenvalues and eigenfunctions for planar acetylene by wave–packet propagation, and its mode–selective infrared excitation. *J. Chem. Phys.*, 107(9):3402–3416, 1997.

[15] R. Chen and H. Guo. Symmetry-enhanced spectral analysis via the spectral method and filter diagonalization. *Phys. Rev. E*, 57(6):7288–7293, 1998.

[16] R. Chen, H. Guo, L. Liu, and J. T. Muckerman. Symmetry–adapted filter diagonalization: Calculation of the vibrational spectrum of planar acetylene from correlation functions. *J. Chem. Phys.*, 109(17):7128–7136, 1998.

[17] R. C. Mowrey and D. J. Kouri. Close–coupling wave packet approach to numerically exact molecule–surface scattering. *J. Chem. Phys.*, 84(11):6466–6473, 1986.

[18] D. J. Kouri and R. C. Mowrey. Close–coupling wave packet formalism for gas phase nonreactive atom–diatom colisions. *J. Chem. Phys.*, 86(4):2087–2094, 1987.

[19] O. A. Sharafeddin and J. C. Light. "Pointwise" versus basis representations for two–dimensional spherical dynamics. *J. Chem. Phys.*, 102(9):3622–3628, 1995.

[20] G. J. Kroes, J. G. Snijders, and R. C. Mowrey. Performance of fully close–coupled wave packet method for the H_2 + LiF(001) model problem. *J. Chem. Phys.*, 103(12):5121–5136, 1995.

[21] G. J. Kroes, J. G. Snijders, and R. C. Mowrey. Performance of close–coupled wave packet method for molecule–corrugated surface scattering. *J. Chem. Phys.*, 102(13):5512–5524, 1995.

[22] C. J. Bradley and A. P. Cracknell. *The Mathematical Theory of Symmetry in Solids.* Clarendon, Oxford, 1972.

[23] J. Manz, P. Saalfrank, and B. Schmidt. Quantum dynamical aspects of rotationally and vibrationally mediated photochemistry in matrices and at surfaces: HCl/DCl in Ar, and NH_3/ND_3 at Cu(111). *J. Chem. Soc. Faraday Trans.*, 93(5):957–967, 1997. see also http://www.rsc.org/is/journals/clic_rsc/net_4.htm.

[24] B. Schmidt. Quantum dynamics of HF photodissociation in icosahedral $Ar_{12}HF$ clusters: Rotational control of the hydrogen atom cage exit. *Chem. Phys. Lett.*, 301(3–4):207–216, 1999.

[25] P. Žďánská, B. Schmidt, and P. Jungwirth. Photolysis of hydrogen chloride embedded in the first argon solvation shell: Rotational control and quantum dynamics of photofragments. *J. Chem. Phys*, 110(13):6246–6256, 1999.

[26] H. Bethe. Termaufspaltung in Kristallen. *Ann. Phys.*, 3(2):132–208, 1929.

[27] J. H. van Vleck. Theory of the variations in paramagnetic anisotropy among different salts of the iron group. *Phys. Rev.*, 41:208–215, 1932.

[28] J. H. van Vleck. The group relation between the Mullikan and Slater–Pauling theories of valence. *J. Chem. Phys.*, 3:803–807, 1935.

[29] L. Pauling. The rotational motion of molecules in crystals. *Phys. Rev.*, 36:430–443, 1930.

[30] A. F. Devonshire. The rotation of molecules in fields of octahedral symmetry. *Proc. Roy. Soc. (London) A*, 153:601–621, 1936.

[31] F. C. von der Lage and H. A. Bethe. A method for obtaining electronic eigenfunctions and eigenvalues in solids with an application to sodium. *Phys. Rev.*, 71(9):612–622, 1947.

[32] S. L. Altmann and A. P. Cracknell. Lattice harmonics. I. Cubic groups. *Rev. Mod. Phys.*, 37(1):19–32, 1965.

[33] S. L. Altmann and C. J. Bradley. Lattice harmonics. II. Hexagonal close–packed lattice. *Rev. Mod. Phys.*, 37(1):33–45, 1965.

[34] F. M. Mueller and M. G. Priestley. Inversion of cubic de Haas–van Alphen data, with an application to palladium. *Phys. Rev.*, 148(2):638–643, 1966.

[35] N. V. Cohan. The spherical harmonics with the symmetry of the icosahedral group. *Proc. Cambridge Phil. Soc.*, 54:28–38, 1958.

[36] A. G. McLellan. Eigenfunctions for integer and half-odd integer values of J symmetrized according to the icosahedral group and the group C_{3v}. *J. Chem. Phys.*, 34(4):1350–1359, 1961.

[37] K. H. Michel. Free energy and orientational phase transition in solid C_{60}. *Z. Phys. B.*, 88:71–78, 1992.

[38] L. Elcoro, J. M. Perez-Mato, and G. Madariaga. Determination of quasicrystalline structures: A refinement program using symmetry–adapted parameters. *Acta Cryst. A*, 50:182–193, 1994.

[39] Y. Zheng and P. C. Doerschuk. Explicit orthonormal fixed bases for spaces of functions that are totally symmetric under the rotational symmetries of a Platonic solid. *Acta Cryst. A*, 52:221–235, 1996.

[40] W. Prandl, P. Schiebel, and K. Wulf. A recursive algorithm for the generation of symmetry–adapted functions: Principles and applications to the icosahedral group. *Acta Cryst.*, A 52:171–175, 1996.

[41] G. W. Fernando, M. Weinert, R. E. Watson, and J. W. Davenport. Point group symmetries and gaussian integration. *J. Comp. Phys.*, 112:282–290, 1994.

[42] R. N. Zare. *Angular Momentum. Understanding Spatial Aspects in Chemistry and Physics.* Wiley, New York, 1987.

[43] F. A. Cotton. *Chemical Applications of Group Theory.* Wiley, New York, 1963.

[44] M. E. Rose. *Elementary Theory of Angular Momentum.* J. Wiley, New York, 1957.

[45] A. R. Edmonds. *Angular Momentum in Quantum Mechanics.* Princeton University, Princeton, 1960.

[46] C. H. Choi, J. Ivanic, M. S. Gordon, and K. Ruedenberg. Direct recurrence relations for the rapid and stable determinaation of rotation matrices between spherical harmonics. *J. Chem. Phys., in press*, 1999.

[47] J. Alvarellos and H. Metiu. The evolution of a wave function in a curve crossing problem computed by a Fast–Fourier–Transform method. *J. Chem. Phys.*, 88(8):4957, 1988.

[48] W. H. Press, S. A. Teukolsky, W. T. Vetterling, and B. P. Flannery. *Numerical Recipes in Fortran.* Cambridge University, Cambridge, 1992.

Appendix: Tables of Seed Functions

The twelve tables in this appendix list the coefficients of seed functions for various representations of the octahedral (O_h) and icosahedral point group (I_h). Note that the tables are complete in the sense that (1) SASHs of arbitrarily high order can be generated accurately and efficiently from these seed functions with the help of the recursive procedure (see Eqs. (23) and (26) in Sec. 3.4) and (2) SASHs for the missing representations of u–symmetry can be supplemented by the use of Eq. (28) in Sec. 4.3. Moreover, the first $500 \times l^{(\Gamma)}$ SASHs for each representation of the two point groups under consideration have been tabulated and can be downloaded from the WWW pages of one of the authors (http://www.zib.de/burkhard.schmidt/SAWP).

The coefficients in the tables refer to real valued combinations of spherical harmonics which are defined as [22]

$$\begin{aligned} \gamma_{jnm}^{(c,\Gamma)} &= \frac{c_{jnm}^{(\Gamma)} + c_{jn-m}^{(\Gamma)}}{\sqrt{2}N}, \quad m \geq 0 \\ \gamma_{jnm}^{(s,\Gamma)} &= \frac{c_{jnm}^{(\Gamma)} - c_{jn-m}^{(\Gamma)}}{i\sqrt{2}N}, \quad m > 0 \end{aligned} \tag{30}$$

where the superscripts 'c' and 's' refer to the cos–like or sin–like ϕ–dependence of the corresponding linear combinations of spherical harmonics and N ensures the correct normalization. Note that the coefficients of the seed functions are given in terms of fractions and square roots of integer numbers to avoid round–off errors when recursively generating higher order functions from the seeds.

The tables are organized similarly to those in Ref. [22]: The first column gives the value of the angular momentum quantum number j. If a degenerate set of SASHs occurs, successive lines for the same j correspond to $n = 1, 2, \cdots, N_j^{(\Gamma)}$. The second column indicates the ϕ–dependence. In some cases the symbol c/s occurs which stands for two functions where the upper and lower plus or minus signs correspond to the cos–like or sin–like function, respectively. The follwing columns are the coefficients γ for various m as defined above. Finally, the last column gives the normalization factor N.

The sets of SASH functions for multi–dimensional irreducible representations can be assigned to $l^{(\Gamma)}$ different subsets, see our explanations in Sec. 4.3. Accordingly, the tabulated seed functions are sometimes split into two or three (H_g) tables according to the different ϕ dependence and/or mutually exclusive sets of numbers m for non–vanishing coefficients $\gamma_{jnm}^{(\Gamma)}$. For example, the third line of Tab. 1 stands for the function

$$Z_{61} = \left(\sqrt{2}Y_{60} - \sqrt{7}(Y_{64} + Y_{6-4})\right)/4 \tag{31}$$

which is the only ($n = 1$) SASH for $j = 6$ which transforms according to the A_{1g} representation of the O_h group.

Octahedral point group (O_h)

Table 1: A_{1g} representation of the octahedral point group (O_h)

j	r	0	4	N
0	c	1		1
4	c	$\sqrt{21}$	$\sqrt{15}$	6
6	c	$\sqrt{2}$	$-\sqrt{14}$	4

Table 2: A_{1u} representation of the octahedral point group (O_h)

j	r	4	8	N
9	s	$\sqrt{102}$	$-\sqrt{42}$	12

Table 3: A_{2g} representation of the octahedral point group (O_h)

j	r	2	6	N
6	c	$\sqrt{11}$	$-\sqrt{5}$	4

Table 4: E_g representation of the octahedral point group (O_h)

j	r	0	4	N
2	c	1		1
4	c	$\sqrt{15}$	$-\sqrt{21}$	6

j	r	2	N
2	c	1	1
4	c	1	1

Table 5: T_{1g} representation of the octahedral point group (O_h)

j	r	1	3	5	7	N
4	c/s	$\mp\sqrt{14}$	$\sqrt{2}$			4
6	c/s	$\mp 2\sqrt{3}$	$-\sqrt{30}$	$\pm\sqrt{22}$		8
8	c/s		$\mp\sqrt{78}$	$-\sqrt{10}$	$\pm 2\sqrt{14}$	12

j	r	4	8	N
4	s	1		1
6	s	1		1
8	s	$\sqrt{130}$	$-\sqrt{14}$	12

Table 6: T_{2g} representation of the octahedral point group (O_h)

j	r	1	3	5	N
2	c/s	1			1
4	c/s	$\pm\sqrt{2}$	$\sqrt{14}$		4
6	c/s	$6\sqrt{913}$	$\mp 5\sqrt{9130}$	$-19\sqrt{498}$	664

j	r	2	6	N
2	s	1		1
4	s	1		1
6	s	$3\sqrt{9130}$	$-13\sqrt{166}$	332

Icosahedral point group (I_h)

Table 7: A_g representation of the icosahedral point group (I_h)

j	r	0	5	10	N
0	c	1			1
6	c	$\sqrt{11}$	$\sqrt{14}$		5
10	c	$\sqrt{741}$	$-3\sqrt{418}$	$\sqrt{1122}$	75

Table 8: A_u representation of the icosahedral point group (I_h)

j	r	5	10	15	N
15	s	$-5\sqrt{1334}$	$2\sqrt{4785}$	$\sqrt{10010}$	250

Table 9: T_{1g} representation of the icosahedral point group (I_h)

j	r	1	4	6	9	11	14	N
6	c/s	$\sqrt{66}$	$\mp\sqrt{22}$	$\sqrt{12}$				10
10	c/s	$\mp\sqrt{494}$	$-3\sqrt{114}$	$\pm 4\sqrt{57}$	$2\sqrt{17}$			50
14	c/s		$-5\sqrt{874}$	$\mp 15\sqrt{23}$	$30\sqrt{22}$	$\pm 2\sqrt{165}$	$\sqrt{15015}$	250

j	r	5	10	N
6	s	1		1
10	s	$-\sqrt{285}$	$2\sqrt{85}$	25
14	s	$-2\sqrt{115}$	$\sqrt{165}$	25

Table 10: T_{2g} representation of the icosahedral point group (I_h)

j	r	2	3	7	8	12	N
8	c/s	$\mp\sqrt{1430}$	$\sqrt{195}$	$\pm 3\sqrt{35}$	$4\sqrt{35}$		50
10	c/s	$\mp\sqrt{442}$	$-8\sqrt{17}$	± 26	$7\sqrt{6}$		50
12	c/s	$-\sqrt{3230}$	$\pm 2\sqrt{4845}$	$8\sqrt{70}$	$\mp 17\sqrt{70}$	$2\sqrt{3795}$	250

j	r	5	10	N
8	s	1		1
10	s	$2\sqrt{85}$	$\sqrt{285}$	25
12	s	$-\sqrt{570}$	$\sqrt{55}$	25

Table 11: G_g representation of the icosahedral point group (I_h)

j	r	1	4	6	9	11	N
4	c/s	$\sqrt{105}$	$\pm 2\sqrt{30}$				15
6	c/s	$\mp 2\sqrt{2}$	$-\sqrt{6}$	$\pm\sqrt{11}$			5
8	c/s	$\sqrt{66}$	$\mp\sqrt{42}$	$-3\sqrt{13}$			15
12	c/s		$\mp 3\sqrt{30198885}$	$-2\sqrt{12434835}$	$\pm 22\sqrt{186990}$	$6\sqrt{29810}$	20325

j	r	2	3	7	8	12	N
4	c/s	$\mp\sqrt{210}$	$\sqrt{15}$				15
6	c/s	$\mp\sqrt{5}$	$2\sqrt{5}$				5
8	c/s	$\pm\sqrt{1155}$	$6\sqrt{70}$	$\mp\sqrt{390}$	$2\sqrt{390}$		75
12	c/s	$\mp 6\sqrt{20132590}$	$-8\sqrt{30198885}$	$\pm 78\sqrt{436310}$	$63\sqrt{436310}$	$\pm 271\sqrt{44715}$	101625

Table 12: H_g representation of the icosahedral point group (I_h)

j	r	1	4	6	9	N
2	c/s	1				1
4	c/s	$2\sqrt{30}$	$\mp\sqrt{105}$			15
6	c/s	$\sqrt{2}$	$\pm 3\sqrt{6}$	$2\sqrt{11}$		10
8	c/s	$\pm 4\sqrt{663}$	$\sqrt{51051}$	$\mp 3\sqrt{374}$		255
10	c/s	$\sqrt{174590}$	$\mp 7\sqrt{40290}$	$-9\sqrt{20145}$	$\pm 4\sqrt{7505}$	1975

j	r	2	3	7	8	N
2	c/s	1				1
4	c/s	$\sqrt{15}$	$\pm\sqrt{210}$			15
6	c/s	$2\sqrt{5}$	$\pm\sqrt{5}$			5
8	c/s	$\mp\sqrt{46410}$	$3\sqrt{85085}$	$\pm\sqrt{2805}$	$-17\sqrt{2805}$	1275
10	c/s	$-3\sqrt{523770}$	$\pm 16\sqrt{20145}$	$58\sqrt{1185}$	$\mp 47\sqrt{790}$	3950

j	r	0	5	10	N
2	c	1			1
4	c	1			1
6	c	$\sqrt{14}$	$-\sqrt{11}$		5
8	c	$-3\sqrt{221}$	$2\sqrt{1309}$		85
10	c	$-\sqrt{1152294}$	$66\sqrt{1343}$	$79\sqrt{4503}$	5925